Available online at www.sciencedirect.com

ScienceDirect

journal homepage: www.elsevier.com/locate/issn/15375110

Research Paper

Testing organic photovoltaic modules for application as greenhouse cover or shading element

Maayan Friman Peretz [a,b], Farhad Geoola [a], Ibrahim Yehia [c], Shay Ozer [a], Asher Levi [a], Esther Magadley [c], Roman Brikman [a], Lavi Rosenfeld [a], Avi Levy [b], Murat Kacira [d], Meir Teitel [a,*]

[a] Institute of Agricultural Engineering, Agricultural Research Organization, The Volcani Center, HaMaccabim Road 68, P.O. Box 15159, Rishon LeZion, 7528809, Israel
[b] Department of Mechanical Engineering, Ben-Gurion University of the Negev, P.O. Box 653, Beer-Sheva, 81405, Israel
[c] Triangle Research and Development Center, P.O. Box 2167, Kfar-Qari, 30075, Israel
[d] Biosystems Engineering, The University of Arizona, Tucson, AZ, 85721, USA

ARTICLE INFO

Article history:
Received 10 December 2018
Received in revised form
11 April 2019
Accepted 17 May 2019
Published online 11 June 2019

Keywords:
Organic materials
Photovoltaic panel
Solar energy
Efficiency
Protected crops

This study examines the feasibility of using semi-transparent, flexible organic photovoltaic (OPV) modules as greenhouse shading material. By using such modules, it may be possible to utilise existing greenhouse-based agricultural areas for electricity production. Using OPV modules to shade greenhouses and reduce excess solar energy may result in reduced heat load on the crop on the one hand, and use of renewable energy on the other. We examined the radiometric and thermal properties of an OPV module. Module transmissivity was measured under outdoor conditions at four different angles of radiation incidence: 0, 21, 41 and 46°. Simultaneously, the open-circuit voltage, and short-circuit current of the module were recorded for power and efficiency calculations. Supplementary laboratory measurements of transmissivity, reflectivity and absorptivity were performed with a spectroradiometer. To further characterise the OPV module, its overall heat-transfer coefficient (*U* value) was determined. The examined module had about 20% transmissivity, 15% reflectivity and 65% absorptance in the photosynthetically active radiation (PAR) range. The mean daily power conversion efficiency of the module was about 0.8% and the overall heat transfer coefficient *U*, was about 6.0 $Wm^{-2}\,K^{-1}$. The temperature of a module placed on the polyethylene cover of a greenhouse high tunnel was about 50–55 °C at midday. Thermal images of the module revealed non-uniform heat distribution, with temperature differences between regions reaching up to 7.5 °C. OPV modules appear to be suitable for greenhouse shading and electricity generation but currently they are too expensive and their life duration is relatively short.

© 2019 IAgrE. Published by Elsevier Ltd. All rights reserved.

* *Corresponding author.*
E-mail address: grteitel@agri.gov.il (M. Teitel).
https://doi.org/10.1016/j.biosystemseng.2019.05.003
1537-5110/© 2019 IAgrE. Published by Elsevier Ltd. All rights reserved.

Nomenclature

A_m	PV module area, m^2
A_w	Area of the insulated walls, m^2
E	Efficiency, %
FF	Fill factor
G	Mean global incident solar radiation, W m^{-2}
I_{sc}	Short-circuit current, A
k_p	Thermal conductivity coefficient of polyurethane, W m^{-1} K^{-1}
k_w	Thermal conductivity coefficient of wood, W m^{-1} K^{-1}
P_{bpp}	Boundary of power production per OPV module area, W m^{-2}
Q	Heat loss through the OPV module, W
Q_H	Heat supplied by the electric heater, W
Q_W	Heat loss through the insulated walls, W
R^2	Coefficient of determination
T	Air temperature, K
U	Global heat-transfer coefficient, W m^{-2} K^{-1}
V_{oc}	Open-circuit voltage, V

Greek letters

α	Absorptance, %
Δx_p	Polyurethane thickness, m
Δx_w	Wooden wall thickness, m
η	Power conversion efficiency, %
λ	Wavelength, nm
ρ	Reflectance, %
τ	Transmittance, %

Abbreviations

AC	Alternating current
BHJ	Bulk-heterojunction
CPM	Conventional planar multi-crystalline silicon module
CPV	Concentrated photovoltaic
DC	Direct current
HOMO	Highest occupied molecular orbital
LUMO	Lowest unoccupied molecular orbital
NIR	Near infrared radiation
OGGH	Off grid greenhouse
OPV	Organic photovoltaic
PAR	Photosynthetically active radiation
PV	Photovoltaic
STM	Semi-transparent PV module
UV	Ultraviolet

1. Introduction

A change in the energy supply to greenhouse farms is needed due to increasing energy prices in the last decade, a scarcity of resources, the steady increase in greenhouse area around the world, and recent policies and regulations in many countries aimed at increasing the use of renewable energy.

Crop yields depend strongly on the availability of light. However, in high-irradiation regions or during the summer, for some crop species, solar radiation can be excessive. Therefore, shading screens and coating applications are used to reduce radiation intensity, making the light level tolerable for crops and reducing energy demand for greenhouse cooling (López-Marin, Gálvez, González, Egea-Gilabert, & Fernández, 2012). The implication is that the excess sunlight irradiating greenhouses can serve to power the operation of environmental control equipment using photovoltaic (PV) films and panels. The use of PV panels in conjunction with agricultural crops has become a popular topic because both are very important in resolving food and energy issues (Marucci, Zambon, Colantoni, & Monarca, 2018).

In recent years, conventional PV panels have become far cheaper, with prices dropping each year. Reported system prices of residential and commercial PV systems declined 6%–7% per year, on average, from 1998 to 2013, and by 12%–15% from 2012 to 2013, depending on system size (Feldman et al., 2014). The price of a module as of October 2018 is in the range of $0.218–0.395 per watt for multi-Si modules producing 270–300 W peak value. The cost of an installed solar PV system as of the first quarter of 2017 was US$2.80 W^{-1} DC or US$3.22 W^{-1} AC for residential systems. For larger commercial systems, it was US$1.85 W^{-1} DC or US$2.13 W^{-1} AC (Fu, Feldman, Margolis, Woodhouse, & Ardani, 2017). In the first half of 2018, the cost of a solar PV system (2.5–10 kW) was US$3.5–4.2 W^{-1} (Feldman & Margolis, 2018).

Greenhouse- and screenhouse-based production systems offer the potential to accommodate PV panels and films as cover materials or integrated into shading screens. However, such technologies need to be studied and evaluated for their ability to generate and transfer energy to the greenhouse systems; their effect on crop growth and yield; and resource-use efficiency, to provide recommendations for growers, system manufactures and greenhouse designers, and to make this integrated technology effective and commercially viable.

1.1. Literature review

Several studies have been performed in last decade to test the application of PV panels in greenhouses. Yano et al. (2009) studied flexible lightweight PV panels mounted on the inside of a north–south oriented greenhouse roof, concluding that the panels with a smaller tilt angle generate more power.

Although the amount of solar radiation was decreased due to the partial shading by PV panels, some crops were found to be morphologically adapted to the conditions, such as lettuce, cucumber, durum wheat and French bean crops (Marrou, Wery, Dufour, & Dupraz, 2012). Furthermore, in crops that generally need high amounts of solar radiation, Kläring and Krumbein (2013), modelling tomato crops subjected to partial shading of PV panels with 57% reduced amount of photosynthetic photon flux density, reported a 50% decrease in plant dry matter. However, their research showed that the dry matter actually decreased by only 31%. In addition to PV panels generating power for greenhouse components, many studies have investigated a hybrid power-generating system. In fact, Quaschning (2004) stated that in areas with high solar irradiation, using a PV-thermal system provides the best value based on initial costs and power-sustaining features.

Sonneveld et al. (2010a) designed and evaluated a greenhouse with linear Fresnel lenses in the cover, acting as a

concentrated PV (CPV) system for power generation. The CPV system retained all direct solar radiation, while diffuse solar radiation passed through into the greenhouse cultivation system. A peak power of 38 W m^{-2} electrical output was obtained at 792 W m^{-2} incoming radiation, and a peak power of 170 W m^{-2} thermal output was obtained at 630 W m^{-2} incoming radiation. Thus, they indicated that incoming direct radiation results in a thermal yield of 56% and an electrical yield of 11%, with a combined efficiency of 67%.

The system dynamics of an off-grid greenhouse (OGGH) production system (140 m^2 greenhouse area) powered by a solar PV power-generation system installed on the side of the greenhouse was evaluated by Juang and Kacira (2014). The study focused on documenting and analysing the resource inputs (water, fertiliser, energy, labour) required for crop production, as well as resource outputs (energy produced, yield) obtained from the integrated production system, and evaluated the system capabilities and limitations. The OGGH was capable of controlling the greenhouse environment at acceptable limits for crop growth. The cherry tomato yield from the OGGH was 0.96 kg m^{-2} $week^{-1}$, and the integrated OGGH produced 19.8 MJ m^{-2} while demanding 18.3 MJ m^{-2} of energy. The water-use efficiency was 0.72 kg l^{-1} and the energy productivity of the greenhouse production system was 269.3 kg MJ^{-1}.

A prototype greenhouse that combines reflection of near-infrared (NIR) radiation with electrical power generation using hybrid PV cell–thermal collector modules was described by Sonneveld, Swinkels, Bot, and Flamand (2010b, c). The reflected NIR radiation was focused with a circular trough by a factor of 30. Besides the generation of electrical and thermal energy, the reflection of the NIR radiation resulted in improved climate conditions in the greenhouse. Under Dutch weather conditions, the yearly produced electrical energy by the prototype was 20 kW h m^{-2} and the yearly thermal yield was 161 kW h m^{-2}. The authors indicated that although the overall efficiency of such a system is relatively low, it can still be attractive due to the large greenhouse areas available in regions with high solar radiation.

In addition to the attempts to use concentrated solar radiation on PV cells, others have also investigated non-concentrated solar radiation with PV systems (Al-Ibrahim, Al-Abbadi, & Al-Helal, 2006; Yano et al., 2009). Al-Ibrahim et al. (2006) examined the potential of using a PV system to power a greenhouse in an arid region in Saudi Arabia. They illustrated the potential harmony between the solar radiation availability and the demand for electricity. Furthermore, they showed that performances of the PV subsystem, battery subsystem and greenhouse cooling system were satisfactory. In particular, the battery system was able to exclusively supply sufficient electrical power to meet the load requirement for over 100 h. Finally, they proved that PV power is a technically viable and adequate option for supplying electrical power to greenhouses in remote areas where electricity from a national electrical grid may not exist.

In a recent study by Yano, Onoe, and Nakata (2014), two prototypes of semi-transparent bifacial PV modules intended for greenhouse roof applications were developed. A module (PV1) using 1500 spherical solar microcells (1.8 mm diameter, crystalline silicon) with 15.4 cell cm^{-2} density in an area of 108×90 mm^2 was produced; 39% of the area was covered with the cells. The remaining 61% was transparent to allow sunlight to enter the greenhouse to guarantee plant photosynthesis. Similarly, a module (PV2) was made using 500 cells with 5.1 cell cm^{-2} density; 13% of the area of this module was covered with the cells. The conversion efficiencies from sunlight energy to electrical energy were 4.5% for the PV1 module and 1.6% for the PV2 module. Calculations of the annual electrical energy production per unit greenhouse land area indicated that these modules are potentially suitable for greenhouses in high-irradiation regions where electricity production may be high.

In another study, Cossu et al. (2016) used a semi-transparent PV module (STM) that was composed of 4800 spherical silicon microcells (1.2 mm diameter) sandwiched between glass plates and integrated into a greenhouse roof with 26.5° slope. The characteristics of the prototype were compared with those of a conventional planar multi-crystalline silicon module (CPM). The module conversion efficiency was steady at around 0.2% over a wide incident angle of sunlight. The yield factor of the STM was slightly higher than that of the CPM because of the isotropic properties of the spherical cells, which were able to use both the sky-incident and ground-reflected irradiation for energy production, irrespective of the module slope.

Variation of shading inside a tunnel prototype greenhouse was analysed (Marucci et al., 2018), by installing PV panels in a checkerboard arrangement. In tunnel greenhouses, due to their curved shape, it is more difficult than in regular multi-span greenhouses to install PV panels on an even part of the cover. The transparent flexible PV panels were manufactured using monocrystalline silicon cells, with an efficiency of 18%, incorporated into polymers with high resistance. The difference and distribution of the shading percentages were examined with respect to the surface area affected by the PV roof, the total area, and the section of the greenhouse. In particular, variations were observed in the percentage of shading and the size of the shaded area. The percentage of shading with the adopted PV arrangement never exceeded 40% during the year.

Trypanagnostopoulos, Kavga, Souliotis, and Tripanagnostopoulos (2017) presented results of energy production and crop performance in a greenhouse with installed PVs. The results were obtained with a lettuce crop. Regarding electrical output, the PV panels produced 50.83 kW h m^{-2} for the characteristic cultivation period of February–April, also creating 20% greenhouse shading. The plant growing results under shading effect were satisfactory, as they were at same level with those of reference greenhouse without PV covered roof.

A study that introduced a novel algorithm to estimate accumulated global radiation inside PV greenhouses was reported by Cossu et al. (2017a). The direct and diffuse radiation were calculated for several observation points inside a PV greenhouse. The algorithm was tested in a greenhouse with 50% PV cover ratio on the roof. The results were presented as the percentage ratio of the accumulated yearly global radiation with and without PV array on the roof, and used to draw maps of light distribution on different canopy heights (from 0.0 to 2.0 m).

The light distribution in a PV greenhouse where the entire roof area was covered with PV panels was reported by Cossu et al. (2017b). The calculation of the incident radiation was estimated under clear sky conditions at several observation points located inside the greenhouse at 1.5 m above ground level. The simulated data were validated through measurements inside a PV greenhouse complex. The global radiation on the greenhouse area was 33% on a yearly basis, compared to the potential value with no PV panels on the roof. The zones close to the gable walls and the south side wall were less shaded than the central region of the greenhouse area.

Colantoni et al. (2018) evaluated climatic conditions inside a greenhouse, in which 20% of the roof surface was replaced with mobile PV panels. The PV system implemented in that study could vary the light energy-collection surface in relation to the degree of insolation. The aim was to observe the shading effects of the PV system on the growth of several varieties of flowers. Results described the distribution of solar radiation, variability of temperature, humidity and lighting, and the observed outcomes on floristic production.

The approaches summarised in this section evaluated PV–greenhouse systems using rigid crystalline silicon and thin-film PV modules. The literature shows that when greenhouse roofs are not completely covered with the PV system, there is nearly no effect on crop yields. Ideally, the target should be to allow maximum usage of the photosynthetically relevant light reaching the plants, while harnessing unused wavelengths for electricity generation.

In photosynthesis, the sun's energy is converted by the plants to chemical energy. However, the various wavelengths in sunlight are not all used equally. Instead, photosynthetic organisms contain light-absorbing molecules called pigments that absorb only specific wavelengths of visible light, while reflecting others. The three key pigments in photosynthesis are chlorophyll *a*, chlorophyll *b*, and β-carotene. Chlorophyll molecules absorb blue and red wavelengths (roughly in the range of 400–470 and 630–680 nm); carotenoids are another key group of pigments that absorb violet and blue-green light.

Organic PV technology (OPV) has advanced in recent years and it appears that it can now be tuned to absorb light that is not required for photosynthesis/growth for power generation, and transmit a spectrum that is beneficial to the crop. The working principle of these PV cells is briefly described in section 1.2.

1.2. *Working principle of organic solar cells*

The working principle of OPV modules and the materials used to manufacture them have been detailed in numerous studies (e.g. Jørgensen et al., 2013; Katz, Gevorgyan, Orynbayev, & Krebs, 2007; Norrman, Larsen, & Krebs, 2006). Here, we provide a brief introduction and report on basic materials used in this technology, for the convenience of the reader.

PV cells work by using the energy of absorbed photons to generate free charge carriers (holes and electrons) which deliver electrical power at the contacts. In OPV cells, this conversion of energy is accomplished using organic materials (Dennler, Scharber, & Brabec, 2009).

The main difference between the working principles of organic and inorganic solar cells is the direct generation of free charge carriers in the latter. In organic materials, the light absorption generates excitons, which become separated at the interface between two different organic layers (heterojunction) (Cornaro & Di Carlo, 2016; Gregg & Hanna, 2003). The material that donates an electron when separating the exciton is called the donor, characterised by a high LUMO (lowest unoccupied molecular orbital), while the material receiving an electron is called the acceptor, and is characterised by a low HOMO (highest occupied molecular orbital). The energy alignment of these two materials is optimised to, on the one hand, efficiently separate the excitons and on the other, prevent energy losses in this process (Kim et al., 2013).

Figure 1 shows the main working principle of OPVs, summarised as follows (Chiechi, Havenith, Hummelen, Koster, & Loi, 2013; Cornaro & Di Carlo, 2016):

1. The absorption of a photon creates an exciton.
2. The exciton migrates to the donor/acceptor interface (heterojunction).
3. A charge-transfer is created between the two materials creating free carriers (positive and negative polarons).
4. The charges diffuse into the bulk materials and are collected at the electrodes (anode and cathode).

The most promising OPV solar cells, in terms of commercial viability, are polymer solar cells, in which the active layer consists of a conjugated polymer as the donor and a fullerene derivative as the acceptor (He et al., 2012). The most common materials used for the active layer are poly (3-hexylthiophene) (P3HT) and phenyl-C61-butyric acid methyl ester (PCBM) (Kalonga, Chinyama, Munyati, & Maaza, 2013). These materials, classified as organic semiconductors, are known for their outstanding optical absorption properties and charge transport characteristics (Heeger, Sariciftci, & Namdas, 2010).

Improvements in OPV performance have been achieved by using different OPV architectures, such as bulk heterojunction (BHJ) and inverted device structures, and by developing low-bandgap conjugated polymers and innovative small organic molecules as donor materials (Cornaro & Di Carlo, 2016).

The main advantages and drawbacks of OPV technology in comparison to silicon PV technology are presented in Table 1. The table considers mainly commercial production and not laboratory production or testing.

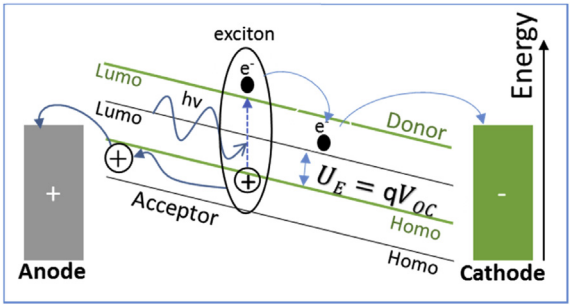

Fig. 1 – A photon with energy $h\nu$ generates an exciton that separates into a positive and negative polaron. The charges are then collected at the electrodes.

Table 1 – Main advantages and drawbacks of OPV in comparison to silicon PV technology.

Silicon PV technology	OPV technology
Expensive manufacturing cost	Potential for low manufacturing cost (roll-to-roll process)
High temperature during fabrication, requires metal or glass support layer	Low-temperature manufacture enables thin transparent plastic film to be used as support layer
Solar cells are usually rigid, heavy and fragile	Solar cells are light, flexible and rugged
Solar cells are generally black or blue	Solar cells can be virtually any colour and semi-transparent
Application mostly limited to planar surfaces	Can be applied to non-planar surfaces
Present efficiency of commercial panels is in the range of about 15–20%	Present efficiency of commercial panels is in the range of about 2–4%
Cost of US$0.4–0.8 W^{-1} (only panel)	Cost of US$15–30 W^{-1} (only panel)
Have 25 years power performance warranties	Degradation of OPVs varies from few weeks to about 2 years.
Have negative temperature coefficients: output decreases with increasing temperature	Positive as well as negative values of temperature coefficients are reported in literature (Belhocine-Nemmar, Belkaid, Hatem, & Boughias, 2010; Bristow & Kettle, 2015; Mehmood et al., 2018; Potscavage, 2011).

1.3. *Recent studies related to OPV application in the rural environment*

Eight different research groups contributed state-of-the-art OPV cells to a study at Pomona College (Owens et al., 2016). Power-conversion efficiency and fill factor (FF) were determined from I–V curves collected at regular intervals over 6–8 months. Similarly, prepared devices were measured indoors, outdoors, and after dark storage. Device architectures were compared. Cells kept indoors performed better than those kept outdoors due to the absence of temperature and humidity extremes. Encapsulated cells performed better due to the minimal oxidation. Some devices showed steady ageing, but many failed due to corrosion of electrodes. Degradation of cells kept in dark storage was minimal over periods of up to 1 year.

Fourteen large-area, flexible, indium tin oxide-free, roll-to-roll processed OPV modules, encapsulated with low-cost materials, were installed on corrugated steel roofs at two sites in a rural village in Southern Rwanda and were continuously monitored (Emmott et al., 2016). This field trial exposed modules to very high levels of insolation, in particular in the ultraviolet (UV) region, with high temperatures and heavy rainfall. The modules exhibited practical life times (to degradation of 20% of their initial capacity) of between 2½ and 5 months, a value 5–6 times lower than control modules kept both in the dark and outdoors in Roskilde, Denmark. Degradation was primarily the result of extensive delamination caused by failure of the non-UV-stable encapsulation, which led to decay in the FF, open-circuit voltage (V_{oc}) and short-circuit current (I_{sc}) of the module.

In a brief review, Yu, Zheng, and Huang (2014) summarised the advances and state-of-the-art performance of OPVs in very recent years. Based on several of the latest developed approaches to accurately detecting the separation of electron–hole pairs in the femtosecond regime, the theoretical interpretation to exploit the comprehensive mechanistic picture of energy harvesting and charge carrier generation was discussed, especially for OPV modules with bulk and multiple heterojunctions. In addition, some approaches to further increasing the efficiency of OPVs were described, including thermotic and dynamic modification methods. Finally, the review highlighted the challenges and prospects of OPVs, with the aim of providing a better understanding toward their high efficiency.

2. Materials and methods

Two types of OPV module (supplied by different manufacturers) were tested in this study, namely module *A* and *B*. Module *A* was manufactured by OPVIUS (Kitzingen, Germany). It was tested in all hereafter described experiments. It was made of few foils assembled into one module using a support material in a lamination process, according to our request. According to the manufacturers' data sheet its efficiency is $\eta = 2.3\%$. Module B was manufactured by Infinity (Jyllinge, Denmark). Due to its smaller size and lower transmissivity compared to module *A* in the photosynthetically active radiation (PAR) range, it was only tested for its spectral radiometric characteristics. Module B is commercially available and has an efficiency η of about 4% according to the manufacturers' data sheet. The active areas (without the edges of the encapsulating material) of modules *A* and *B* were 0.560 m^2 and 0.238 m^2, respectively, and their dimensions were 0.655 m × 0.855 m and 1 m × 0.238 m, respectively.

2.1. *Spectral radiometric characteristics*

Solar radiation is characterised by a wide range of wavelengths that can be divided into defined ranges: UV (<400 nm), PAR (400–700 nm), NIR (700–2500 nm) and IR (>2500 nm). The most important range for agricultural purposes is the PAR range, used by plants for photosynthesis. However, the other ranges may also be important through their influence on pollinating bees and beneficial insects that are often used in greenhouse cultivation, on plant morphogenesis and on other plant– and canopy–environment interactions.

The spectral characteristics (transmittance (τ), reflectance (ρ) and absorptance (α)) of the OPV module were determined using a spectroradiometer (LI-1800, LiCOR, Nebraska, USA) with an integrating sphere in the wavelength range of 390–1100 nm at 2 nm resolution. Transmittance and reflectance as a function of wavelength were measured with the spectroradiometer and absorptance, was calculated using Eq. (1).

$$\alpha(\lambda) = 1 - [\tau(\lambda) + \rho(\lambda)] \quad (1)$$

Three repetitions in each of the different regions (see Fig. 2) of the OPV module were used to determine its average spectral transmittance and reflectance. The average spectral

transmittance and reflectance were calculated using a weighted average, considering the percent area of each region out of the total area of the module.

2.2. Determination of mean transmittance at different radiation-incidence angles

The transmissivity of module A was also measured under field conditions using a transmittance-measuring box (partially based on ASTM E 424-71 (2015)) (Fig. 3). The 1.2 m × 0.6 m base and 0.2 m high side walls of the box were made of treated wood, painted matte black and divided into two equal cells. One cell was covered by an OPV module and the other was left open and served as a reference for the measurements of incident radiation. Incident solar radiation was measured by a pyranometer (Li-200R, LiCOR, Lincoln, NB, USA). Transmissivity of the OPV was calculated from radiation values measured below the module divided by values of incident radiation. The OPV module is a heterogeneous material that has regions of different spectral characteristics. To obtain an average value that takes into account the different regions in the module (see Fig. 2), nine Li-200R pyranometers (a grid of 3 × 3, see Fig. 3) each with a wavelength range of 400–1100 nm were organised in the middle of the cell at the bottom of the box. The distance between adjacent sensors in a line of the grid was 0.075 m.

Greenhouse roofs in the Mediterranean region are generally convex, due to the extensive use of flexible films as cover material. Thus, at a given time during the day, different angles of incident solar radiation are expected at different points on the greenhouse cover. Therefore, transmissivity of the flat OPV module was examined at different sun incident angles: 0, 22, 41 and 46°, by rotating the box about a horizontal axis. Zero degrees indicated sun rays perpendicular to the OPV module. Three repetitions were done for each incident angle. To examine whether the orientation of the module strips relative to solar rays affects the results, several sets of measurements were performed with module strips perpendicular to the rotation axis (see Fig. 3) and in other sets, the strips were parallel; these are hereafter referred to as lengthwise and widthwise orientation of the module, respectively.

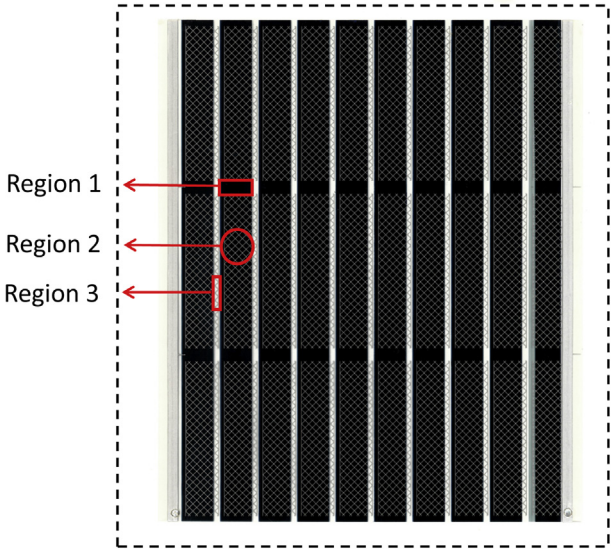

Fig. 2 – Sample of OPV module A with its different regions. The dashed line on the circumference indicates the edges of the transparent lamination material. The 10 black module strips are vertical. Region 1 is 6.2% of the total area, region 2 is 73.8%, and region 3 is 20%.

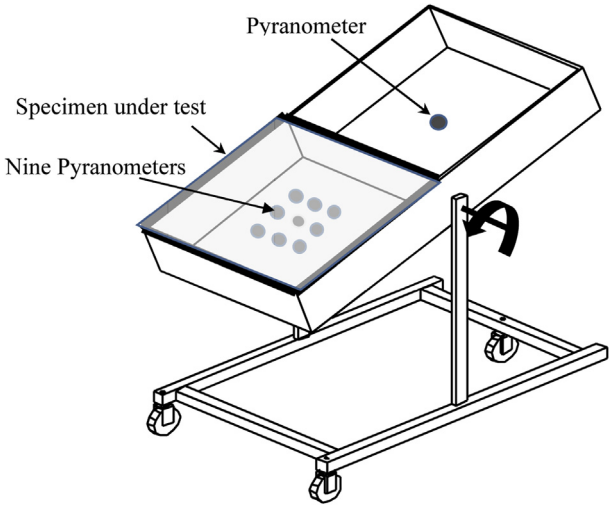

Fig. 3 – Schematic diagram of transmittance measuring box.

The output of each pyranometer was recorded at a rate of 1 Hz using a CR1000 data logger (Campbell Scientific, Logan, UT, USA) to which an AM25T multiplexer (Campbell Scientific, Logan, UT, USA) was connected. Averages of all nine sensors were calculated for periods of 30 s and used for data analysis. All measurements were taken under clear sky conditions at midday. Air temperature, relative humidity and wind speed were measured by a standard meteorological station and during the experiment, their values were 25.5 °C, 28–47% and 2.5–4.5 m s^{-1} respectively.

2.3. Electricity production of the OPV module

Electricity production and efficiency of the OPV module were measured at the same four angles of sun incidence (0, 22, 41 and 46°). Similar to the experiments in which the average transmittance was determined, several sets of measurements were performed, in which the module strips were parallel or perpendicular to the rotation axis. For each angle of sun incidence, V_{oc} and I_{sc} were measured by a multimeter and the boundary of power production per OPV module area (P_{bpp}) and, efficiency (E) were calculated as:

$$P_{bpp} = \frac{V_{oc} \cdot I_{sc}}{A_m} \left[Wm^{-2}\right] \quad (2)$$

$$E = \frac{P_{bpp}}{G} \cdot 100 \ [\%] \quad (3)$$

where A_m is the OPV module area and G [W m^{-2}] is the mean global incident solar radiation at the time when voltage and current were measured.

2.4. Fill factor and power conversion efficiency

While the product of V_{OC} and I_{sc} mark the boundaries of power production in a solar cell, the maximum power produced Pmax occurs at the voltage Vmax and current-density Imax where the product of I and V is at maximum absolute value. Because of resistance and losses, |Imax| and Vmax are always less than $|I_{SC}|$ and V_{OC}, respectively. The fill factor FF describes these differences and is defined as (Potscavage, 2011):

$$FF = \frac{I_{max}\, V_{max}}{I_{sc}\, V_{oc}} \tag{4}$$

FF is an indication of how close Imax and Vmax come to the boundaries of power production of I_{SC} and V_{OC}. Since higher FF is related to higher maximum power, high FF is desired.

The power conversion efficiency η is defined as the percentage of incident solar radiation that is converted into output power when the solar cell is connected to a load.

$$\eta = E \cdot FF = \frac{I_{sc}\, V_{oc}\, FF}{A_m G} \tag{5}$$

To evaluate the electrical output of the OPV panel that was placed on a greenhouse tunnel roof, the electrical behaviour of a module was monitored throughout the day. Current–voltage (I–V) curves were recorded every 10 min using a Keithley 2460 Source-meter (Tektronix, Inc. Beaverton, OR, USA) and the irradiance in the respective plane of the panel was measured at the same time using EKO ML-02 pyranometers (EKO Instruments Co., Tokyo, Japan). From the I–V curves, open circuit voltage V_{oc}, and short-circuit current I_{sc}, were found, as well as the maximum power point P_{max}, fill factor FF, and efficiency η.

2.5. Value of the overall heat-transfer coefficient U of the OPV module

The overall heat-transfer coefficient of the OPV module, U, was determined by using a standard hot box. The U value takes into account the heat transfer through the module by radiation, convection and conduction and can be calculated from:

$$U = \frac{Q}{A_m(T_{in} - T_{out})} \quad [Wm^{-2}K^{-1}] \tag{6}$$

where Q is the amount of heat loss through the OPV module and T_{in} and T_{out} are the air temperatures in the hot box and outside of it, respectively ($T_{in} > T_{out}$).

The hot box was a cube with dimensions of $1 \times 1 \times 1$ m^3 with five walls made of 0.01-m thick wood and the sixth face left open. The five walls were insulated with 0.1-m thick polyurethane to minimise heat loss. The OPV module was installed on the open face of the cube so that heat could be transferred mainly through this face. To generate a temperature difference between the inner space of the cube and the environment, an electric heater was placed at the bottom of the box and used to heat the air. The heating power of the electric heater was adjusted between 30 and 300 W with a voltage regulator, and the respective input power was measured with a wattmeter. The temperatures inside and outside the box were measured by thermocouples of 0.51-mm diameter wires.

Experiments were performed at night only under clear sky conditions, for 2 weeks. Every night, a different temperature difference was set by changing the power supply to the heater. For each test, steady-state conditions prevailed from 04:00–05:00 h. Calculations were performed using only data of steady-state heat transfer through the OPV module. Losses through the insulated box walls were taken into account by subtracting heat loss through the five insulated walls from the heat supplied by the electric heater:

$$U = \frac{Q_H - Q_w}{A_w(T_{in} - T_{out})} \quad [Wm^{-2}K^{-1}] \tag{7}$$

where Q_H is the heating power and Q_w is the heat loss through the five insulated walls. The heat loss through the walls was calculated from:

$$Q_w = A_w\left(\frac{k_w}{\Delta x_w} + \frac{k_p}{\Delta x_p}\right)(T_{in} - T_{out}) \tag{8}$$

where $k_w = 0.055$ [W m^{-1} K^{-1}] at 300 K and $k_p = 0.022$ [W m^{-1} K^{-1}] at 300 K are the thermal conductivity coefficients of wood and polyurethane, respectively, A_w [m^2] is the area of the five insulated walls and Δx_p and Δx_w [m] are the thicknesses of the polyurethane and wood, respectively.

Temperatures, input power of the electric heater, wind velocity and ambient relative humidity were recorded every minute by the CR1000 data logger. During the tests, the mean wind velocity above the OPV module was about 1 m s^{-1} and the mean ambient temperature and mean relative humidity were about 12 °C and 85%, respectively.

In addition to the above described experiments, the temperature of module A which was placed on a polyethylene cover of a greenhouse high tunnel was recorded over several days (7–9 July 2018) simultaneously with the temperature of the polyethylene sheet adjacent to the module. Tomato plants were grown in the tunnel when the measurements were performed. The temperatures were measured by very fine thermocouple wires (0.127 mm) attached to the OPV module and polyethylene from below. In addition, thermal photos of the module were taken by a thermal camera (I5, FLIR® Systems Inc., OR, USA) on 25 Sep 2018 at about 08:45 h local time.

3. Results and discussion

All presented results refer to module A, unless otherwise stated. Figure 4 shows the solar radiation transmittance of the OPV module for different incidence angles and the two different orientations of the module strips: lengthwise and widthwise. Transmissivity decreased as the incidence angle increased, as expected. With solar radiation perpendicular to the module (0° incident angle), transmissivity in the wavelength range 400–1100 nm was slightly higher than 27%. At an incident angle of 46°, the transmissivity decreased to about 22%. Transmissivity was higher with widthwise vs. lengthwise orientation. The difference in transmissivity between the two orientations increased systematically as the incident angle increased (Fig. 4).

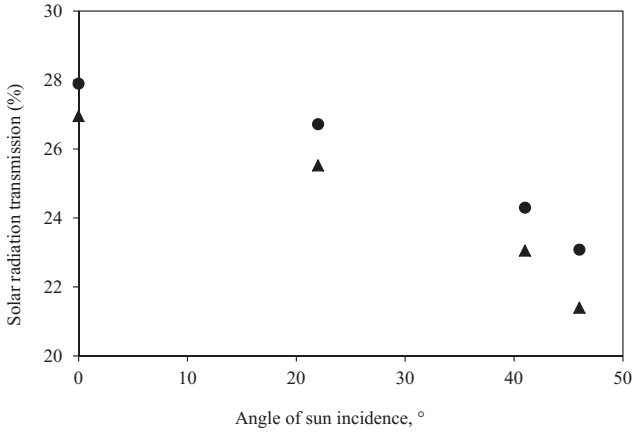

Fig. 4 – Solar radiation transmission of OPV module at different angles of sun incidence. ▲, Lengthwise; •, Widthwise.

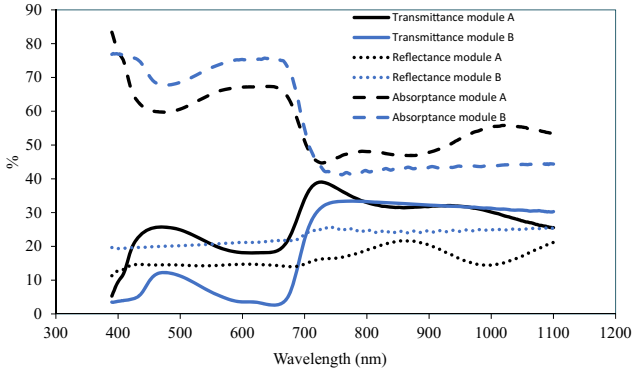

Fig. 6 – Transmittance, reflectance and absorption spectra of OPV modules A and B. Values are weighted averages of all three regions in module A (similar weighted averages were done with module B).

The spectral transmittance of region 2 of four A modules is presented in Fig. 5. The measurements were performed on samples taken from four randomly chosen modules. There were differences in the spectral transmittance, which were pronounced at wavelengths higher than 700 nm. Up to 700 nm, the shape of the transmittance curves were very similar in all samples and only the absolute value of transmittance at a given wavelength changed among the samples. Above 700 nm, the shape of the curves changed and transmittance peaks were observed at different wavelengths, apparently due to inherent differences in the manufacturing process of the modules. Modules 1 and 2 had very similar transmittance above 700 nm, whereas in modules 3 and 4, the transmittance and the wavelength at which a peak was observed differed from those in modules 1 and 2 (Fig. 5).

Figure 6 shows the transmittance, reflectance and absorptance spectra of OPV modules A and B obtained from measurements with the LI-1800 spectroradiometer. Note that the figure shows the weighted average of all three regions of the module. OPV module A had a high absorptance with low reflectance. The highest absorptance values were observed in the range of 400–650 nm. At about 660 nm, there was a sharp decrease in absorptance from 66 to 45%. Between 700 and 900 nm, the absorptance values were roughly constant (45–48%) (Fig. 6). Transmittance values changed between 5 and 40% with two peaks: a broad peak at a wavelength of 460–470 nm where transmittance was about 25%, and another peak at 730 nm where transmittance was about 40% (Fig. 6). Reflectance values were roughly constant and equal to about 15% over the range of 400–700 nm. At wavelengths higher than 700 nm, the reflectance increased and reached a peak of value 21% at about 870 nm, then began to decrease (Fig. 6).

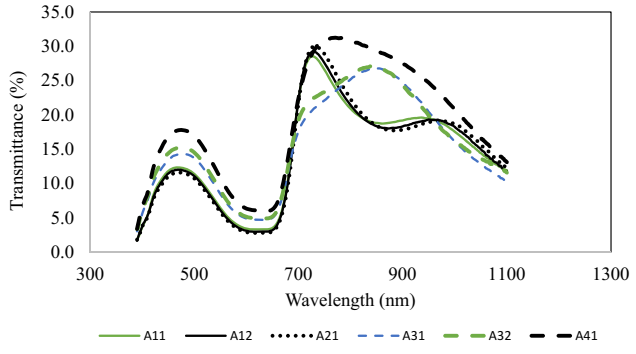

Fig. 5 – Radiation transmission of region 2 of module A, at different wavelengths. The figure shows data obtained from different modules from the same manufacturer. The first number in the sample name represents the module number and the second number represents the repeat number.

Overall, the behaviour of OPV module B was similar to that of module A (Fig. 6). Module B had higher absorptance at 400–650 nm and lower absorptance in 700–1100 nm compared to module A. The reflectance of module B was fairly constant over the range 400–1100 nm, at about 20–25%, which is 7% higher than that of module A. In the wavelength range of 400–700 nm, module B had a much lower transmittance than module A and at wavelengths above 800 nm, both modules had almost the same transmittance (Fig. 6).

The average transmittance, reflectance and absorptance of both modules A and B in the wavelength range of 390–1100 nm and 400–700 nm (PAR range) are presented in Table 2.

In hot climates with high radiation levels, greenhouses are often equipped with a shading screen to reduce internal solar radiation levels. From Table 2, it can be seen that in the wavelength range of 390–1100 nm, the transmittance of modules A and B was equivalent to 72.9% and 79.1% shading. Therefore, it can be concluded that partial coverage of a greenhouse by OPV modules can reduce the entry of excess solar energy and thus reduce the heat load on the crop without the use of shading screens. Although this is an advantage in the summer time, during the winter, when solar radiation is much lower, this could be a drawback, since sufficient solar radiation, especially in the PAR range which is important for plant growth, might not enter the greenhouse.

The current commercially available modules seem to have high radiation absorptance in the wavelength range of 400–700 nm, capturing the energetic photons in this range to generate electricity; this, in turn, reduces the amount of light

Table 2 – Average transmittance, reflectance and absorptance of the OPV modules A and B.

Wavelength range (nm)	Transmittance (%)		Reflectance (%)		Absorptance (%)	
	Modules		Modules		Modules	
	A	B	A	B	A	B
390–1100	27.1	20.9	16.3	23.0	56.6	56.1
400–700	21.4	7.1	14.4	20.7	64.2	72.2

reaching the canopy. It is thus suggested that future modules be designed to use more of the IR range of the spectrum (>700 nm) to generate electricity, thereby improving transmittance in the PAR range which is critical for plant growth.

The boundary of power production per OPV module area of OPV module A at four angles of sun incidence 0, 22, 41 and 46° is presented in Table 3. For all angles of sun incidence and module orientations, the voltage remained quite constant at about 28.0–28.6 V. The boundary of power production per OPV module area decreased as the sun incidence angle increased; this decrease was mainly observed when the incident angle changed from 22 to 41° (Table 3).

Negligible changes were observed when the incident angle changed from 0 to 22° and from 41 to 46°. The efficiency E remained relatively constant, in the range of 1.9–2.2%. There was practically no difference in power output or efficiency between lengthwise and widthwise orientations (Table 3).

The values of the measured overall heat-transfer coefficient, U, as a function of $\Delta t = T_{in} - T_{out}$ of module A, are presented in Fig. 7. All U values had standard deviations of less than 0.1 W m^{-2} K^{-1}. The U value remained fairly constant in a Δt range of about 10–35 °C, with an average value of 6 W m^{-2} K^{-1}. The U value for glass greenhouses (Papadakis et al., 2000) is 4–8 W m^{-2} K^{-1} and for polyethylene greenhouses, 4–16 W m^{-2} K^{-1} (Papadakis et al., 2000; Feuilloley & Issanchou, 1996; Geoola, Kashti, Levi, & Brickman, 2009, 2011). It should be noted that the wind speed in present tests was relatively low, 1 ms^{-1}. At higher wind speeds, the value of U is expected to increase.

In polyethylene-covered greenhouses, costly moveable shading and thermal screens are often used to either reduce heat load on the greenhouse or heat loss from it. The screens reduce the overall U value of the greenhouse cover (Geoola et al., 2009, 2011). The OPV module had a U value similar to that of glass with good thermal properties. Therefore, the use of OPV modules as part of a polyethylene greenhouse cover may result in energy-saving with respect to greenhouse heating during the winter, possibly eliminating the need to use thermal screens.

The diurnal change in P_{bpp} generated by a module placed at the apex of a greenhouse high tunnel is shown in Fig. 8, together with the incident solar radiation. The incident solar radiation and P_{bpp} were well correlated. In the early hours, when solar radiation was low, P_{bpp} was low as well. The value of P_{bpp} increased toward noon with the increase in solar radiation. At 06:30 h, the solar radiation was about 70–100 W m^{-2} and P_{bpp} was about 2 W m^{-2}; at noon, the solar radiation increased to 950–1000 W m^{-2} and the module produced 12.5–13.5 W m^{-2}. After noon radiation and P_{bpp} decreased simultaneously. It appears that at 18:00 h, when the solar intensity was similar to that at 06:30 h, the value of P_{bpp} was higher than at 06:30 h.

The change in P_{bpp} of the module that was placed on the roof of the tunnel, as function of the incident solar radiation is shown in Fig. 9. A linear curve was fitted to the data points and it was forced to pass through zero. The equation of the curve was $y = 0.0147x$ and the value of the coefficient of determination, $R^2 = 0.612$. The mean daily module efficiency E (calculated from the value of the slope of the best–fit curve) was equal to 2.6%. It is noted that the experimental data (not shown) indicated that E decreased towards midday and increased towards the afternoon.

The change in FF as function of incident solar radiation is shown in Fig. 10. The figure shows that the values of FF changed in the range of 0.24–0.38. The value of the FF decreased with solar radiation, except in the range $G < 100$ where it increased with radiation. Figure 10 shows that there is a hysteresis in the change of FF during the day, apparently due to an hysteresis in the module temperature. Temperature data of an OPV module (not shown) indicated a clear diurnal hysteresis. For a given incident solar radiation, with an increase in radiation towards midday, the values of FF were lower than with a decrease in radiation towards evening. The values of FF in this study are much lower than those obtained with small OPV cells, 0.72–0.76 (Jao, Liao, & Su, 2016), since the modules in this study were much larger than laboratory scale cells. It is known from literature that an increase in the size of the module reduces the value of the FF and hence the value of η. The mean daily power conversion efficiency η was equal to about 0.8%. This value is much lower than the one reported for small scale laboratory OPV cells, 17.3% (Meng et al., 2018).

It is anticipated that under OPV efficiencies of 1–2%, for an area of 1 ha, it is possible to get in Israel, on a yearly basis, about 2.4×10^5 kW h. A 1 ha greenhouse will need 40 fans each consuming about 1.3 kW h for about 6 h a day on a yearly basis (1.12×10^5 kW h). Thus, the energy produced by the OPV modules is more than twice required by the fans. Hence, the roof can only partially be covered by OPV modules to allow higher light penetration into the greenhouse and still have electricity to operate fans, pumps, electric motors and other actuators that use much less energy than fans. Alternatively, electricity can be sold by feeding the electric grid.

Figure 11 shows, for 3 consecutive days, the temperatures of the greenhouse polyethylene 150 μm film directly underneath an OPV module (we assume it adequately represents the temperature of the module) and the polyethylene cover adjacent to an OPV module without an OPV module on top of it. It also shows ambient air temperature and incident solar radiation. The OPV module was much warmer than the

Table 3 – Boundary of power production per OPV module area and efficiency of OPV module A.

Angle	G (W m^{-2})		V_{oc} (V)		I_{sc} (mA)		P (Wm^{-2})		E (%)	
	Lengthwise	Widthwise	Lengthwise	Widthwise	Lengthwise	Widthwise	Lengthwise	Widthwise	Lengthwise	Widthwise
0	880	914	28.0	28.0	376.0	390.0	18.5	19.2	2.1	2.1
22	859	868	28.6	28.0	376.1	388.5	18.9	19.1	2.2	2.2
41	710	731	28.3	28.2	287.0	282.1	14.2	13.9	2.0	1.9
46	659	657	28.4	28.2	291.3	279.7	14.5	13.8	2.2	2.1

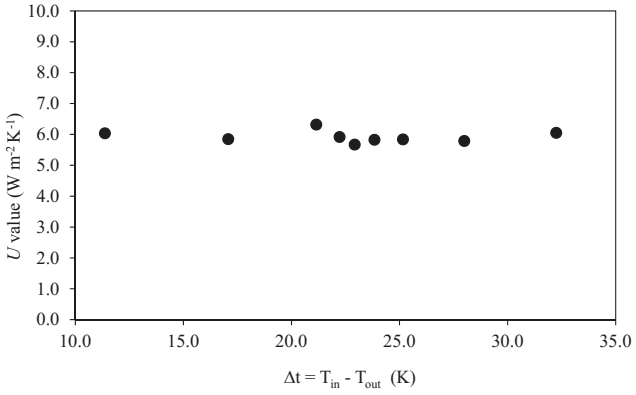

Fig. 7 – Measured *U* values of OPV module *A*.

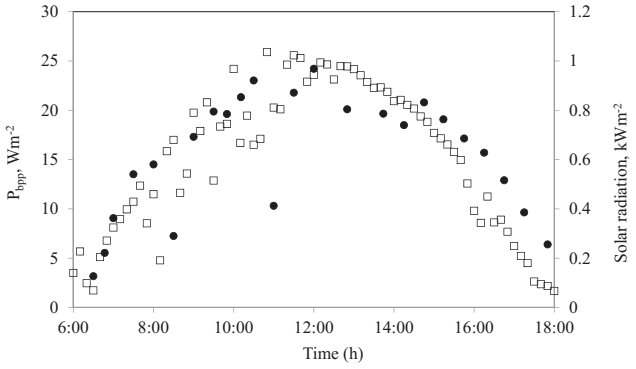

Fig. 8 – Diurnal change in boundary of power production per OPV module area (Pbpp) of a module that was placed on the apex of a greenhouse high tunnel. □, Incident solar radiation; •, P_{bpp}.

polyethylene. At noon, the temperature of the OPV module was in the range of 51–53 °C, whereas the polyethylene temperature was in the range 34–35 °C. The polyethylene was about 2 °C warmer than the ambient air. During the

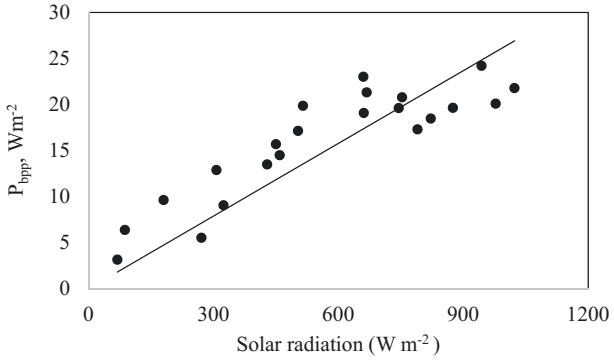

Fig. 9 – Change in boundary of power production per OPV module area (P_{bpp}) as a function of incident solar radiation. Solid line represents linear regression, y = 0.0263x, R^2 = 0.612.

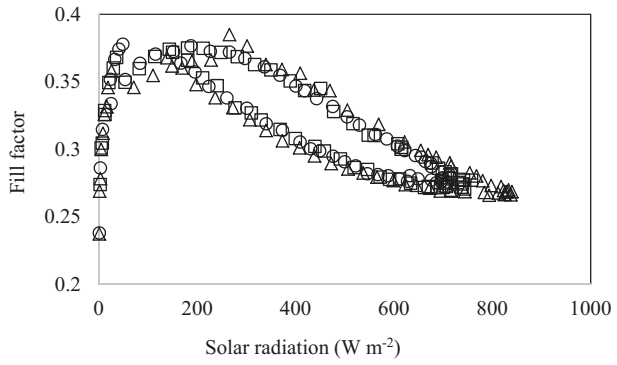

Fig. 10 – Fill factor of module A as function of solar radiation in three different days with clear sky (□, DOY 300; ○, DOY 311; and Δ, DOY 321).

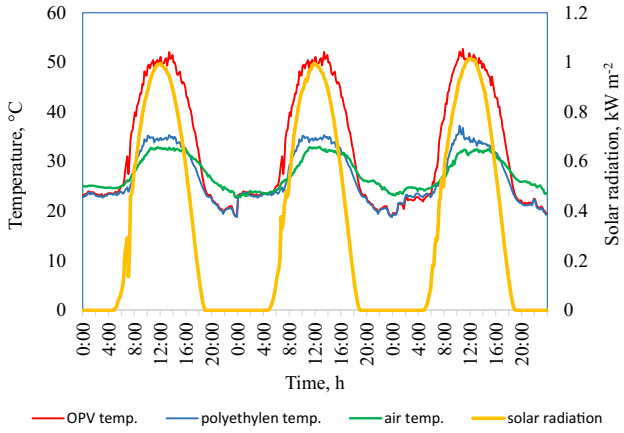

Fig. 11 – Temperatures of an OPV module placed on the greenhouse cover together with temperature of polyethylene adjacent to the module, ambient air temperature and incident solar radiation on three consecutive days, 7–9 July 2018.

night, the temperature of the OPV module was nearly the same as that of the polyethylene, in the range of 19–24 °C. The very high temperature of the OPV module during the day was apparently the main reason for the reduction in efficiency observed towards midday. Mehmood et al. (2018) and Belhocine-Nemmar et al. (2010) indicated that the decrease in efficiency due to an increase in temperature, can be attributed to a decrease in the V_{oc} of the cells. In present study, however, V_{oc} remained nearly constant throughout the day.

Figure 12 shows a thermal image of module A on the apex outside of a high tunnel greenhouse. The module temperature was not uniform, with differences of up to 7.4 °C between different points. This value was recorded under a solar radiation of about 700 W m^{-2}. Larger differences might be expected under higher solar radiation intensity. The minimum and maximum temperatures of the module were 40.9 and 48.3 °C, respectively, and the average temperature of the entire module area was 45.3 °C. Note that the laminating material of the module was at a lower temperature (purple colour) and the polyethylene cover on which the module was placed was much cooler (deep purple/black) than the module. We notice that the fact that the polyethylene was partially transparent to IR in the range of 7–15 μm did not significantly affect the measured polyethylene temperature. It was assumed that the non-uniformity in the temperature distribution could be due to either non-homogeneous fabrication and assembly of the module materials or differences in contact between different regions of the module with the polyethylene sheet on which it was placed. Another possible cause might be module deterioration owing to fluctuations of the polyethylene due to wind forces, which result in slight repeating twists of the module.

4. Summary and conclusions

The currently available dimensions of semi-transparent flexible OPV modules are too small to serve as greenhouse cover

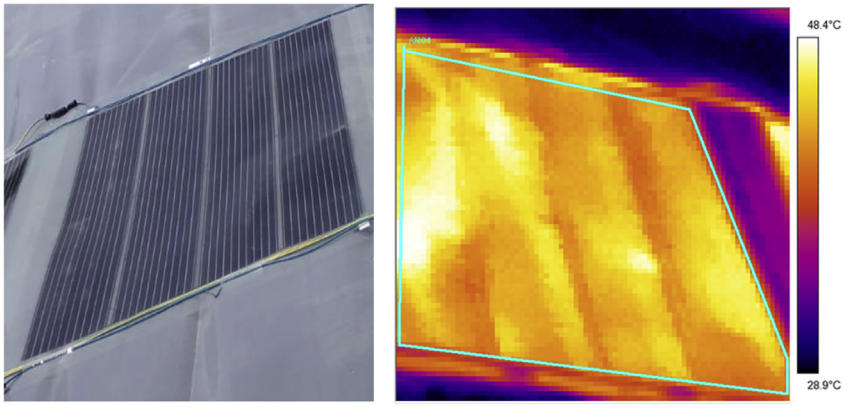

Fig. 12 – OPV module. (a) Image of module on cover of greenhouse high tunnel. (b) Thermal image of module on cover of greenhouse high tunnel. Yellow colour represents OPV module area. Purple/black colour on top and bottom of the photo represents the polyethylene cover of the tunnel on which the module was placed. Purple colour on right side of the module represents the laminating material of the OPV module.

material. Furthermore, the average value of solar radiation transmittance in the PAR region of the spectrum of the present OPV modules, 22–26%, is relatively low for greenhouse applications. However, they can be used as shading elements when placed on conventional greenhouse cover materials and cover only part of the roof, to prevent a too high shading. Radiation transmittance in the IR range is relatively high (about 30%) for greenhouse applications in warm climates, where the desire is generally to reduce the penetration of IR radiation into the greenhouse and thus reduce greenhouse overheating. Attempts should be made to produce modules that convert a larger percentage of the IR spectrum into electricity. The overall heat-transfer coefficient, U, of the module was about 6 W m^{-2} K^{-1}, similar to 4-mm thick greenhouse glass (about 6 W m^{-2} K^{-1}) and lower than that of a polyethylene sheet (7–10 W m^{-2} K^{-1}). The electrical efficiency of the module calculated using the boundary of power production ($V_{oc} \cdot I_{sc}$) per OPV module area, under field conditions was about 2.0–2.6%. The fill factor changed during the day in the range of 0.24–0.38. Thus, the mean daily power conversion efficiency η was equal to about 0.8%, much lower than with commercial silicon modules (15–20%). Absorption of solar radiation by the OPV module resulted in its heating to a temperature of 50–55 °C at midday. Furthermore, the temperature of the module was not uniform, with differences of about 7.5 °C between different points on the module area. The high temperature reached by the OPV module presumably affected its electricity production and reduced its efficiency, E. The effects of OPV shading on plant performance and greenhouse microclimate warrant further study.

Acknowledgements

The authors thank the Chief Scientist of the Ministry of Agriculture and Rural Development of Israel (grant no. 20-12-0027, the BARD, The United States - Israel Binational Agricultural Research and Development fund (grant no. US-4885-16) and the Plant Production & Marketing Board of Israel (grant no. 459-4540-17) for their support.

REFERENCES

Al-Ibrahim, A., Al-Abbadi, N., & Al-Helal, I. (2006). PV greenhouse system-system description, performance and lesson learned. *Acta Horticulturae, 719*, 251–264.

ASTM E 424-71. (2015). *Standard test methods for solar energy transmittance and reflectance (terrestrial) of sheet materials*.

Belhocine-Nemmar, F., Belkaid, M. S., Hatem, D., & Boughias, O. (2010). Temperature effect on the organic solar cells parameters. *International Journal of Chemical and Molecular Engineering, 4*(4), 257–259.

Bristow, N., & Kettle, J. (2015). Outdoor performance of organic photovoltaics: Diurnal analysis, dependence on temperature, irradiance, and degradation. *Journal of Renewable and Sustainable Energy, 7*(1), 013111.

Chiechi, R. C., Havenith, R. W. A., Hummelen, J. C., Koster, L. J. A., & Loi, M. A. (2013). Modern plastic solar cells: Materials, mechanisms and modelling. *Materials Today, 16*(7–8), 281–289.

Colantoni, A., Monarca, D., Marucci, A., Cecchini, M., Zambon, I., Di Battista, F., et al. (2018). Solar radiation distribution inside a greenhouse prototypal with photovoltaic mobile plant and effects on flower growth. *Sustainability, 10*, 855. https://doi.org/10.3390/su10030855.

Cornaro, C., & Di Carlo, A. (2016). Organic photovoltaics for energy efficiency in buildings. *Nano and Biotech Based Materials for Energy Building Efficiency*, 321–355.

Cossu, M., Ledda, L., Deligios, P. A., Sirigu, A., Murgia, L., Pazzona, A., et al. (2017b). Solar light distribution inside a greenhouse with the roof area entirely covered with photovoltaic panels. *Acta Horticulturae, 1182*, 47–55.

Cossu, M., Ledda, L., Urracci, G., Sirigu, A., Cossu, A., Murgia, L., et al. (2017a). An algorithm for the calculation of the light distribution in photovoltaic greenhouses. *Solar Energy, 141*, 38–48.

Cossu, M., Yano, A., Li, Z., Onoe, M., Nakamura, H., Matsumoto, T., et al. (2016). Advances on the semi-transparent modules based on micro solar cells: First integration in a greenhouse system. *Applied Energy, 162*, 1042–1051.

Dennler, G., Scharber, M. C., & Brabec, C. J. (2009). Polymer-Fullerene Bulk-Heterojunction solar cells. *Advanced Materials, 21*, 1323–1338.

Emmott, C. J. M., Moia, D., Sandwell, P., Ekins-Daukes, N., Hösel, M., Lukoschek, L., et al. (2016). In-situ, long-term operational stability of organic photovoltaics for off-grid applications in Africa. *Solar Energy Materials and Solar Cells, 149*, 284–293.

Feldman, F., Barbose, G., Margolis, R., James, T., Weaver, S., Darghouth, N., et al. (2014). *Photovoltaic system pricing trends: Historical, recent, and near-term projections*. US Department of Energy. NREL/PR-6A20-62558.

Feldman, F., & Margolis, R. (2018). *Q1/Q2 2018 Solar industry update*. US Department of Energy. NREL/PR-6A20-72036.

Feuilloley, P., & Issanchou, G. (1996). Greenhouse covering materials measurement and modelling of thermal properties using the hot box method, and condensation effects. *Journal of Agricultural Engineering Research, 65*, 129–142.

Fu, R., Feldman, D., Margolis, R., Woodhouse, M., & Ardani, K. (2017). *U.S. Solar photovoltaic system cost benchmark: Q1 2017*. US Department of Energy. NREL/TP-6A20-68925.

Geoola, F., Kashti, Y., Levi, A., & Brickman, R. (2009). A study of the overall heat transfer coefficient of greenhouse cladding materials with thermal screens using the hot box method. *Polymer Testing, 28*, 470–474.

Geoola, F., Kashti, Y., Teitel, M., Levi, A., Brickman, R., & Esquira, I. (2011). A study of U value of greenhouse films with thermal screens using the hot box method. *Acta Horticulturae, 893*, 367–372.

Gregg, B. A., & Hanna, M. C. (2003). Comparing organic to inorganic photovoltaic cells: Theory, experiment , and simulation. *Journal of Applied Physics, 93*(6), 3605–3614.

Heeger, A. J., Sariciftci, N. S., & Namdas, E. B. (2010). *Semiconducting and metallic polymers*. Oxford UK: Oxford University Press.

He, Z., Zhong, C., Su, S., Xu, M., Wu, H., & Cao, Y. (2012). Enhanced power-conversion efficiency in polymer solar cells using an inverted device structure. *Nature Photonics, 6*, 591–595.

Jao, M. H., Liao, H. C., & Su, W. F. (2016). Achieving a high fill factor for organic solar cells. *Journal of Materials Chemistry A, 4*, 5784–5801.

Jørgensen, M., Carlé, J. E., Søndergaard, R. R., Lauritzen, M., Dagnæs-Hansen, N. A., Byskov, S. L., et al. (2013). The state of organic solar cells -A meta analysis. *Solar Energy Materials and Solar Cells, 119*, 84–93.

Juang, P., & Kacira, M. (2014). System dynamics of a photovoltaic integrated greenhouse. *Acta Horticulturae, 1037*, 99–104.

Kalonga, G.,, Chinyama, G. K., Munyati, M. O., & Maaza, M. (2013). Characterization and optimization of poly (3- hexylthiophene-2, 5- diyl) (P3HT) and [6, 6] phenyl-C61- butyric acid methyl ester (PCBM) blends for optical absorption. *Journal of Chemical Engineering and Materials Science, 4*(7), 93–102.

Katz, E. A., Gevorgyan, S., Orynbayev, M. S., & Krebs, F. C. (2007). Out-door testing and long-term stability of plastic solar cells. *The European Physical Journal Applied Physics, 36*, 307–311.

Kim, B. G., Ma, X., Chen, C., Ie, Y., Coir, E. W., Hashemi, H., et al. (2013). Energy level modulation of HOMO, LUMO, and band gap in conjugated polymers for organic photovoltaic applications. *Advanced Functional Materials, 23*, 439–445.

Kläring, P., & Krumbein, A. (2013). The effect of constraining the intensity of solar radiation on the photosynthesis, growth, yield and product quality of tomato. *Journal of Agronomy and Crop Science, 199*, 351–359.

López-Marin, J., Gálvez, A., González, A., Egea-Gilabert, C., & Fernández, J. A. (2012). Effect of shade on yield, quality and photosynthesis-related parameters of sweet pepper plants. *Acta Horticulturae, 956*, 545–552.

Marrou, H., Wery, J., Dufour, L., & Dupraz, C. (2012). Productivity and radiation use efficiency of lettuces grown in the partial shade of photovoltaic panels. *European Journal of Agronomy, 44*, 54–66.

Marucci, A., Zambon, I., Colantoni, A., & Monarca, D. (2018). A combination of agricultural and energy purposes: Evaluation of a prototype of photovoltaic greenhouse tunnel. *Renewable and Sustainable Energy Reviews, 82*, 1178–1186.

Mehmood, U., Irfan Malik, M., Ul Haq Khan, A., Hussein, I. A., Harrabi, K., & Al-Ahmed, A. (2018). Effect of outdoor temperature on the power-conversion efficiency of newly synthesised organic photosensitiser based dye-sensitised solar cells. *Materials Letters, 220*, 222–225.

Meng, L., Zhang, Y., Wan, X., Li, C., Zhang, X., Wang, Y., et al. (2018). Organic and solution-processed tandem solar cells with 17.3% efficiency. *Science, 361*, 1094–1098.

Norrman, K., Larsen, N. B., & Krebs, F. C. (2006). Lifetimes of organic photovoltaics: Combining chemical and physical characterisation techniques to study degradation mechanisms. *Solar Energy Materials and Solar Cells, 90*, 2793–2814.

Owens, C., Ferguson, G. M., Hermenau, M., Voroshazi, E., Galagan, Y., Zimmermann, B., et al. (2016). Comparative indoor and outdoor degradation of organic photovoltaic cells via inter-laboratory collaboration. *Polymers, 8*, 1–8.

Papadakis, G., Briassoulis, D., Scarascia Mugnozza, G., Vox, G., Feuilloley, P., & Stoffers, J. A. (2000). Radiometric and thermal properties of, and testing methods for, greenhouse covering materials. *Journal of Agricultural Engineering Research, 77*, 7–38.

Potscavage, W. J., Jr. (2011). *Physics and engineering of organic solar cells* (Ph. D. thesis). USA: Georgia Institute of Technology.

Quaschning, V. (2004). Technical and economical system comparison of photovoltaic and concentrating solar thermal power systems depending on annual global irradiation. *Solar Energy, 77*, 171–178.

Sonneveld, P. J., Swinkels, G. L. A. M., van Tujl, B. A. J., Janssen, H. J. J., Campen, J., & Bot, G. P. A. (2010a). Performance of a concentrated photovoltaic energy system with static linear fresnel lenses. *Solar Energy, 85*, 432–442.

Sonneveld, P. J., Swinkels, G. L. A. M., Bot, G. P. A., & Flamand, G. (2010b). Feasibility study for combining cooling and high grade energy production in a solar greenhouse. *Biosystems Engineering, 105*, 51–58.

Sonneveld, P. J., Swinkels, G. L. A. M., Campen, J., van Tuijl, B. A. J., Janssen, H. J. J., & Bot, G. P. A. (2010c). Performance results of a solar greenhouse combining electrical and thermal energy production. *Biosystems Engineering, 106*, 48–57.

Trypanagnostopoulos, G., Kavga, A., Souliotis, M., & Tripanagnostopoulos, Y. (2017). Greenhouse performance results for roof installed photovoltaics. *Renewable Energy, 111*, 724–731.

Yano, A., Furue, A., Kadowaki, M., Tanaka, T., Hiraki, E., Miyamoto, M., et al. (2009). Electrical energy generated by photovoltaic modules mounted inside the roof of a north–south oriented greenhouse. *Biosystems Engineering, 103*, 228–238.

Yano, A., Onoe, M., & Nakata, J. (2014). Prototype semi-transparent photovoltaic modules for greenhouse roof applications. *Biosystems Engineering, 122*, 62–73.

Yu, J., Zheng, Y., & Huang, J. (2014). Towards high performance organic photovoltaic cells: A review of recent development in organic photovoltaics. *Polymers, 6*, 2473–2509.